Inertial Sensors and Their Applications

Inertial Sensors and Their Applications

Jussi Collin, Pavel Davidson, Martti Kirkko-Jaakkola, and Helena Leppäkoski

Abstract Due to the universal presence of motion, vibration, and shock, inertial motion sensors can be applied in various contexts. Development of the microelectromechanical (MEMS) technology opens up many new consumer and industrial applications for accelerometers and gyroscopes. The multiformity of applications creates different requirements to inertial sensors in terms of accuracy, size, power consumption and cost. This makes it challenging to choose sensors that are suited best for the particular application. In addition, development of signal processing algorithms for inertial sensor data require understanding on the physical principles of both motion generated and sensor operation principles. This chapter aims to aid the system designer to understand and manage these challenges. The principles of operation of accelerometers and gyroscopes are explained with examples of different applications using inertial sensors data as input. Especially, detailed examples of signal processing algorithms for pedestrian navigation and motion classification are given.

Jussi Collin
Laboratory of Pervasive Computing, Tampere University of Technology, Finland
e-mail: jussi.collin@tut.fi

Pavel Davidson
Laboratory of Automation and Hydraulics, Tampere University of Technology, Finland
e-mail: pavel.davidson@tut.fi

Martti Kirkko-Jaakkola
Finnish Geospatial Research Institute, National Land Survey, Finland
e-mail: martti.kirkko-jaakkola@nls.fi

Helena Leppäkoski
Laboratory of Automation and Hydraulics, Tampere University of Technology, Finland
e-mail: helena.leppakoski@tut.fi

1 Introduction to Inertial Sensors

Inertial sensors measure motion parameters with respect to the inertial space. They generally fall into two categories: (a) instruments sensing linear inertial displacement, also known as accelerometers, (b) rotational inertial rate sensors, also called angular rate sensors or gyroscopes.

1.1 Accelerometers

An accelerometer is a device that measures translational acceleration resulting from the forces acting on it. This acceleration is associated with the phenomenon of weight experienced by a mass that resides in the frame of reference inside accelerometer and can be described by Newton's second law of motion: "A force **F** acting on a body of mass *m* causes the body to accelerate with respect to inertial space." A typical accelerometer consists of a small mass, also known as a proof or seismic mass, connected via a spring to the case of the instrument as shown in Fig. 1.

When the instrument experiences acceleration along its sensitive axis, the proof mass is displaced with respect to the case of instrument; this is the scenario in Fig. 1b. Under steady state conditions, the force acting on the mass will be balanced by the tension in the spring. The extension (or contraction) of the spring creates a force which is proportional to the displacement. When there is no drag force to resist the movement of the proof mass, its displacement is directly proportional to the acceleration. This way the applied acceleration can be measured by measuring the displacement of the proof mass.

There are many different designs for accelerometer but most of them operate in a manner similar to the simple spring and mass system described above. In many applications, including navigation, the three dimensional vector of acceleration is required. Normally, three single-axis accelerometers are used. In recent years, tri-axis instruments have become very popular in the segment of low-cost accelerometers.

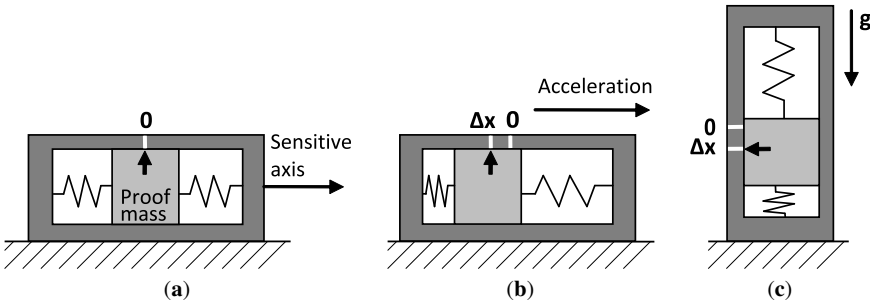

Fig. 1 A mass-and-spring accelerometer under different conditions: (**a**): at rest or in uniform motion; (**b**) accelerating; (**c**) at rest

It is a common practice to mount the three accelerometers with their sensitive axes mutually orthogonal, although any non-coplanar configuration is acceptable as long as the angles between the sensitive axes are known.

Accelerometers are insensitive to the gravitational acceleration and unable to separate the total acceleration from that caused by the presence of a gravitational field [18]. These sensors instead provide measurements of the difference between the true acceleration and the acceleration due to gravity. This quantity is the non-gravitational force per unit mass exerted on the instrument, and often called a specific force. For example, if we consider an accelerometer in free fall, the case and the proof mass will fall together. Therefore, there will be no displacement of the proof mass with respect to the case and the output of the instrument will remain at zero. In other words, the acceleration $\mathbf{a}$ of the instrument with respect to an inertially fixed set of axes equals the gravitational acceleration $\mathbf{g}$ and the specific force is zero. If the accelerometer is held stationary, i.e. $\mathbf{a} = \mathbf{0}$, it will measure the force which is counteracting to stop it from falling, $\mathbf{f} = -m\mathbf{g}$, as visualized in Fig. 1c. This specific force is required to offset the effect of gravitational attraction. Therefore, the measurements provided by the accelerometer must be combined with knowledge of the gravitational field in order to determine the acceleration of the sensor unit with respect to the inertial space.

The various accelerometer technologies include [60]: mechanical, surface acoustic waves, piezoelectric, fiber optic, vibrating beam and solid-state microelectromechanical (MEMS) accelerometers. Historically, mechanical accelerometers were the first type of accelerometers in mass production. All mechanical accelerometers are mass–spring type sensors. They can be implemented in open loop when a displacement of a proof mass with respect to its 'null' position is proportional to the specific force applied along its input axis. They can be also implemented as closed loop or force feedback pendulous accelerometer in which the spring is replaced by an electromagnetic device that produces force on the proof mass to maintain it at its 'null' position. The most precise mechanical force-feedback pendulous accelerometers are capable of measuring specific force with resolutions of micro-g or better. This class of mechanical accelerometers is used in very accurate (navigation grade) inertial navigation systems (INS).

Most of accelerometers nowadays are manufactured using MEMS technology that was developed for the military and aerospace markets in the 1970s. In 2016, the production volume of MEMS inertial sensors was about 7.5 billion units, dominated by consumer electronics and automotive applications. MEMS accelerometers can be fabricated in many different ways. The basic process modules include bulk micromachining, surface micromachining, wafer bonding, and deep reactive-ion etching (DRIE). In most cases, the fabrication involves a combination of two modules or more. The majority of the commercial accelerometers are surface micromachined. One advantage of surface micromachining is its potential of Complementary Metal-Oxide-Semiconductor (CMOS) integration. However, due to some technical challenges, two-chip solutions are still dominant in commercial products. Bulk micromachining is often combined with wafer bonding (glass–silicon or silicon–silicon) to produce high-performance accelerometers. A recent development in which sin-

gle crystal silicon (SCS) sensing elements are created in CMOS substrate by using DRIE shows some promising results. In terms of materials, almost all MEMS accelerometers are made of silicon including silicon on insulator (SOI). More about MEMS accelerometers can be found in [20, Chapter 2.05].

1.2 Gyroscopes

Gyroscope (or gyro for short) is a device for measuring or maintaining angular orientation. It can measure turn rates caused by changes in attitude with respect to inertial space. Historically the first sensors of this kind were mechanical gyros. They exploit the inertial properties of a wheel spinning at high speed, which tends to keep the direction of its spin axis due to the principles of conservation of angular momentum. Although the axle orientation does not remain fixed, it changes in response to an external torque much less and in a different direction than it would without the large angular momentum associated with the disc's high rate of spin and moment of inertia. Since external torque is minimized by mounting the device in gimbals, its orientation remains nearly fixed, regardless of any motion of the platform on which it is mounted. There are several designs for mechanical gyros including: dynamically tuned gyroscope (DTG), flex gyro, and dual-axis rate transducer (DART) which is suitable only for low accuracy applications [60].

Following the development of spinning mass gyros, other kinds of angular rate sensors, such as optical and vibrating gyros, were developed [4]. These sensors are based on different physical principles than the conservation of angular momentum. Optical gyros are based on the Sagnac effect which causes a phase shift between two waves counter-propagating in a ring interferometer that is rotating; the shift is proportional to the rate of rotation. Vibrating gyros are based on Coriolis effect that induces a coupling between two resonant modes of a mechanical resonator. Optical gyros can be effectively implemented using different integrated optics technologies that generally fall into two categories: (a) ring laser gyroscopes (RLG) and (b) fiber optics gyroscopes (FOG). RLGs can be made very accurate to meet the requirements for navigation grade, but on the other hand, they are expensive, their size increases with performance, and they are high-voltage devices. FOGs are less accurate compared to RLGs, but they meet the requirements of medium accuracy (tactical grade), medium cost gyroscopes.

Vibrating gyros are usually manufactured using MEMS technology [20, Chapter 2.06]. From the accuracy point of view, MEMS gyros are of low to medium accuracy with their performance approaching FOG. They have low manufacturing costs, small physical size, and low power consumption; moreover, they can survive severe shocks and temperature changes. Therefore, MEMS technology is ideally suited for mass production.

1.3 Areas of Application

Due to the universal presence of motion, vibration, and shocks, inertial sensors can be applied almost everywhere, from aircraft and space navigation to underground drilling, from hard disk fall protection to airbags in vehicles, and from video games to performance improvement of athletes. The large variety of applications creates different requirements to inertial sensors in terms of accuracy, size, power consumption, and cost. For example, the principal driving force for high-accuracy inertial sensors development has been inertial navigation for aircraft and submarines, precise aiming of telescopes, imaging systems, and antennas. For some applications, improved accuracy is not necessarily the most important issue, but meeting performance at reduced cost and size is. The major requirements to inertial sensors in automotive industry are low cost, high reliability, and possibility of mass production. In the following sections some examples of applications are given.

1.3.1 Navigation

An INS normally consists of three gyros and three accelerometers. The data from inertial sensors is processed to calculate the position, velocity, and attitude of the vehicle. Given the ability to measure the acceleration it would be possible to calculate the change in velocity and position by performing successive mathematical integrations of the acceleration with respect to time. In order to navigate with respect to the desired reference frame, it is necessary to keep track of the direction in which the accelerometers are pointing. Rotational motion of an INS with respect to the inertial reference frame may be sensed by gyroscopes that are used to determine the orientation of the accelerometers at all times. Given this information it is possible to resolve the accelerations into the reference frame before the integration process takes place.

High performance INSs require accurate sensors. Such systems are expensive, weigh several kilos, and have significant power consumption. However, not in every navigation application has a high-performance INS to be used. For example, land vehicle navigation systems can significantly reduce INS error growth by applying non-holonomic constraints[1] and using odometer measurements. Therefore, in many land vehicle applications a lower cost tactical grade INS can be used instead of a more expensive navigation grade INS. Pedestrian navigation systems take advantage of biomechanics of walking. Recognizing that people move one step at a time, the pedestrian mechanization restricts error growth by propagating position estimates in a stride-wise fashion, rather than on a fixed time interval. Inertial sensors are used to detect the occurrence of steps, and provide a means of estimating the distance and direction in which the step was taken. For step detection, accelerometers do not

[1] In short, non-holonomic constraints limit the lateral and vertical speeds of the vehicle and this knowledge is translated into a measurement [53].

have to be of high accuracy. Pedestrian navigation is addressed more profoundly in Sect. 3.

1.3.2 Automotive

In modern cars, MEMS accelerometers are used in airbag deployment systems to detect a rapid negative acceleration of the vehicle, determine if a collision occurred, and estimate the severity of the collision. Another common automotive use of MEMS gyros and accelerometers is in electronic stability control systems. It compares the driver's intended direction which can be determined through the measured steering wheel angle to the vehicle's actual direction determined through measured lateral acceleration, vehicle yaw rotation, and individual wheel speeds.

Other automotive applications of MEMS accelerometers include monitoring of noise, vibration, harshness, and conditions that cause discomfort for drivers and passengers and may also be indicators of mechanical faults. Once the data has been collected during road tests it can be analyzed and compared to previous captures or against donor vehicles. Comparing data may highlight a problem within the vehicle allowing the technician to proceed to a repair with confidence supported by measurements taken.

1.3.3 Industrial

In industrial applications accelerometers are widely used to monitor machinery vibrations. Analysis of accelerometer based vibration data allows the user to detect conditions such as wear and tear of bearings, shaft misalignment, rotor imbalance, gear failure, or bearing fault in rotating equipment such as turbines, pumps, fans, rollers, compressors, and cooling towers. The early diagnosis of these faults can prevent costly repairs, reduce downtime, and improve safety of plants in such industries as automotive manufacturing, power generation, pulp and paper, sugar mills, food and beverage production, water and wastewater, hydropower, petrochemistry, and steel production.

1.3.4 Consumer Products

The availability of small size tri-axis accelerometers and gyroscopes with prices less than $2 has opened up new markets for inertial sensors in video game controllers, mobile phones, cameras, and other personal electronic devices. The applications of inertial sensors in consumer devices can be divided into the following categories: (a) orientation sensing, (b) gesture recognition, (c) motion input, (d) image stabilization, (e) fall detection, and (f) sport and healthy lifestyle applications.

The most common application of orientation sensing by accelerometers is converting the display to a horizontal or vertical format based on the way the device

is being held. For example STMicroelectronics LSM6DSL inertial module provide configurable interrupts for change in orientation [59]. Third-party developers have created thousands of motion-sensitive games and other fanciful applications with orientation sensing features. With the use of the Global Positioning System (GPS) and a magnetic compass, location-based services are enabled, making it possible to identify special sales or lunch menus by just pointing a cell phone at a building.

Computer or video games can exploit gesture recognition techniques and make it possible to play the games or do virtual activities such as swinging a tennis racket or drive a vehicle by moving a hand-held controller. Nintendo's Wii video game console uses a controller called a Wii Remote that contains a tri-axis accelerometer and was designed primarily for motion input. The Sony PlayStation 4 uses the DualShock 4 remote with embedded inertial module that can be used, for example, to make steering more realistic in racing games.

Commonly used example of motion input application is darkening the display when not needed by detecting the motionless state. Some smartphones use accelerometers for user interface control, for example, make selections by scrolling down a list by tilting. The accelerometer-enabled wireless mouse makes it possible to move an object in space and have a corresponding object or cursor follow in a computer-generated visual model.

Cameras use inertial sensors for image stabilization to reduced blurring associated with the motion of a camera during exposure [24]. It compensates for angular yaw and pitch movement of the camera. There are two ways for images stabilization in cameras: (1) make adjustments to the image sensor or the lenses to ensure that the image remains as motionless as possible, (2) digital image stabilization in which the physical image is allowed to track the scene on the sensor by software to produce a stable image. The digital technique requires the pixel count to be increased to allow the image to move on the sensor while keeping reference points within the boundaries of the capture chip. Different companies have different names for their image stabilization technology: Image Stabilizer (Canon), Vibration Reduction (Nikon), Optical SteadyShot (Sony Cyber-Shot), Super SteadyShot (Sony), MEGA Optical Image Stabilizer (Panasonic and Leica), Optical Stabilizer (Sigma), Vibration Compensation (Tamron) and Shake Reduction (Pentax).

Fall detection is an important safety feature to protect hard disk drives in laptops and some other portable, "always on" devices like MP3 players [1]. Many of these devices feature an accelerometer which is used to detect drops. If a drop is detected, the heads of the hard disk are parked to avoid data loss and possible head or disk damage caused by the shock.

1.3.5 Sport

The advent of small low-cost inertial sensors caused the boom in sensor-laden sport equipment. Examples of MEMS inertial sensor application in sports include running, golf, tennis, basketball, baseball, soccer, boxing. Wearable electronics for running may include accelerometers, gyroscopes, magnetometer and pressure sensor

located in waistband, running shorts or footpod. It can measure different running metrics, such as cadence, step length, braking, foot contact time, pelvic rotation, tilt, etc.

In ball games such as soccer and basketball inertial sensors are integrated in the ball. In soccer the equipment estimates how hard the ball has been struck, its speed, spin, and flight path [41]. In basketball the system detects shots made and missed as well as throw distance, speed, spiral efficiency, and whether a ball has been caught or dropped. In bat-and-ball games (baseball, softball, cricket) the equipment is embedded in the bat and computes different swing metrics, including power, speed, efficiency, and distance the bat travels in the hitting zone. In tennis the inertial sensors are usually embedded in rackets handle and they can detect the type of shot (forehand, backhand, serve, and smash), ball spin (topspin, slice), swing speed and ball impact spot. In golf the sensors are attached to the shaft of a club and track the position, speed, and angle of the club as it moves through a swing.

Concussion detection is important in contact sports of all kinds, especially in boxing, football and hockey [47]. MEMS accelerometers that are able to measure more than 100 g are usually embedded in helmets, headbands or mouth guards to measure the severity of an impact. In boxing a small device containing accelerometer can be attached to the boxer hand wraps or gloves to measure punch types and rate, power, hit/miss ratio.

Other examples of inertial sensors in sport include motion analysis such as figure skating jumps, and trajectory analysis in ski jumping and javelin. Xsens MVN Motion Capture [51, 67] is an interesting example of how inertial sensors can be used to record human movement. The motion capture suit includes 17 inertial trackers strapped to the different parts of the body. The data can be used in medical and sports applications to analyze human movement and gait. It can be also used to animate digital characters in movies, games, and virtual environments.

2 Performance of Inertial Sensors

Selection of the most suitable inertial sensors for a particular application is a difficult task. Among the parameters that have to be considered are resolution, dynamic range, accuracy, cost, power consumption, reliability, weight, volume, thermal stability, and immunity to external disturbances. Usually when sensors are examined for compliance, accuracy is the first parameter to start with; however, accuracy cannot be expressed as a single quantity because several factors contribute to it.

All accelerometers and gyros are subject to errors which limit their accuracy in the measurement of the applied acceleration or angular rate. The measurement error is defined as the difference between the measured and the true value of the physical quantity. Generally, inertial sensor errors fall into two broad categories: (a) systematic errors and (b) random errors. When measurement errors are analyzed, the same methodology can be applied to gyros and accelerometers.

Systematic errors are measurable and sensor type specific. They are caused by inaccuracy of system parameters and parasitic effects, streaming from the sensor design, its fabrication processes, and the readout electronics. In the context of MEMS sensors, systematic errors apply to whole batches of sensors of a certain type produced by the same process.

Random errors are caused by interference, noise, instability etc. They can be divided into two groups: (a) wideband or uncorrelated noise and (b) colored or correlated noise. Examples of uncorrelated noise are thermal noise [39] and quantization errors in the analog-to-digital conversion of the output signal. These errors can be modeled as additive Gaussian white noise process. The effect of zero-mean white noise can be mitigated by averaging the signal over longer periods of time; since the output rate of inertial sensors is typically very high (e.g., 1000 Hz), the signals are usually down-sampled to a slower update rate by averaging.

Correlated noise is a more complicated and much more diverse phenomenon. Some examples of correlated noise are random walk, Markov processes, and flicker noise. Flicker or $1/f$ noise is a nonstationary, long-memory process (i.e., its autocorrelation decays slower than exponentially) [34]. The name stems from the fact that the power spectral density of $1/f$ noise is inversely proportional to the frequency; this implies that a major part of the power of the noise is located at low frequencies. In the context of inertial sensors, this noise process is also referred to as bias instability [28], but in this chapter, we will use the term $1/f$ noise to refer to this process and reserve the term "bias instability" for characterizing sensor quality (see Section 2.1).

$1/f$ noise has been observed in a wide range of different contexts, such as semiconductors, time standards, and highway traffic; even the ancient records of river Nile's flood levels have a $1/f$ power spectral density [64]. However, the origin of the phenomenon is not known, but it seems that there is no common physical mechanism to cause it in all these contexts [34]. Therefore, in order to model inertial sensor errors accurately, the contribution of $1/f$ noise must be handled carefully. A common tool for characterizing the contributions of the different noise types is the Allan variance which is described in Section 2.1.2. Other characterization methods do exist [37], but using Allan variance is recommended in [29].

2.1 Effect of Different Sources of Error

When analyzing the measurement errors of inertial sensors, it is a common practice to split the measurement error into several components that are mutually independent and specific to different modes of operation. For instance, even if the applied input signal is absent, the sensor output is not zero; this error source is called an offset or *bias*. Therefore, the bias is defined as the average of sensor output over a specified time interval that has no correlation with the input signal. Accelerometer bias is measured in m/s^2 or fractions of g whereas gyro bias is measured in $^\circ$/h or $^\circ$/s. In many cases the bias is not exactly constant but changes slowly in time.

This phenomenon is also called *bias instability* and can be quantified as the peak-to-peak amplitude of the long-term bias drift.

The next important error component is the *scale factor error* which is defined as the error in the ratio relating the change in the output signal to a change in the applied input signal. Scale factor error is commonly expressed as a ratio of output error to input rate in parts per million (ppm), or, especially in the lower performance class, as a percentage figure.

Cross-axis sensitivity errors result from the sensor's sensitivity to signals applied about axes that are perpendicular to the sensitive axis. Such errors can be due to physical misalignments of the sensors' sensitive axes or, particularly in the case of MEMS sensors, electromagnetic interference between the channels. The cross-axis sensitivity is also expressed in ppm or a percentage of the applied acceleration or angular rate. *Linearity* (non-linearity) error is defined as the closeness of the calibration curve to a specified straight line. The *acceleration-dependent bias* (g-dependent bias) is an error which occurs in Coriolis vibratory gyros; it is proportional to the translational acceleration of the sensor. Sudden impacts and shocks may cause significant errors in the output of both accelerometers and gyroscopes in other ways as well, e.g., as a hysteresis effect.

All the error sources mentioned above consist of both systematic and random errors.

2.1.1 Calibration of Inertial Sensors

Calibration refers to correcting a measuring device by adjusting it to match reference values. Calibration of inertial sensors can significantly improve their performance. Long-term errors, i.e., those which remain constant for at least 3–5 years, can be corrected for in the factory. The factory calibration usually includes temperature compensation to guarantee good performance over the entire operational temperature range. This calibration eliminates a significant part of the measurement errors. The residual errors are much smaller than the initial errors and can be explained by the fact that the bias and scale factor errors can slightly change when the system is turned on next time – the so-called *day-to-day* error. Furthermore, the temperature compensation does not eliminate all errors caused by temperature variations.

Despite the fact that the residual errors are much smaller than the errors before the factory calibration, the sensors' performance can be improved even further if these residual errors are calibrated out. The approach for calibration of these errors depends on the application, the measurement scenario, and the type of error. From the system's perspective, one can approach the errors and their correction based on the sensor transfer characteristic (static and dynamic). With the emergence of digital signal processing and its use with sensors, this approach is becoming the standard. Keeping in mind that all sources of measurement error cumulatively affect the accuracy and resolution of a sensing system in a negative manner, the systems obey the principle of "a chain only being as strong as its weakest link". Errors such as in-

terference, noise, and instability could be eliminated through chopping or dynamic amplification and division applied to individual sensors.

2.1.2 Allan Variance

Named after Dr. David W. Allan, the Allan variance [2] is a quantity to characterize the stability of oscillator systems. Although originally developed for frequency standards, the Allan variance is widely used to characterize the performance of inertial sensors; it reveals the contributions of uncorrelated and random walk type error processes on the measurement noise. The Allan variance σ_A^2 is a function of the averaging time τ, computed as

$$\sigma_A^2(\tau) = \frac{1}{2(N-1)} \sum_{i=1}^{N-1} (\bar{y}_\tau(i+1) - \bar{y}_\tau(i))^2 \tag{1}$$

where the data y have been partitioned into N disjoint bins of length τ, and $\bar{y}_\tau(i)$ is the average value of the ith such bin. The square root of Allan variance is known as the Allan deviation, which is in accordance with common statistical terminology.

Usually, the Allan variance function is visualized as a log–log graph; an example is shown in Fig. 2. Generally, the Allan variance curve is U-shaped. At short averaging times, quantization and uncorrelated noise dominate the output. The variance of independent and identically distributed data is inversely proportional to the averaging time, which causes a negative slope to the Allan variance at short averaging times. As the averaging time increases, after some point, $1/f$ noise starts to dominate over uncorrelated noise and the curve levels off – the Allan variance of $1/f$ noise is constant [64]. Eventually, the curve starts to increase due to rate random walk. There are also other phenomena that can be identified using Allan variance [29], but the three effects discussed above are usually the most significant.

Based on the Allan variance plot, it is possible to quantify certain characteristics of the sensor noise. The spectral density of white noise can be estimated as the

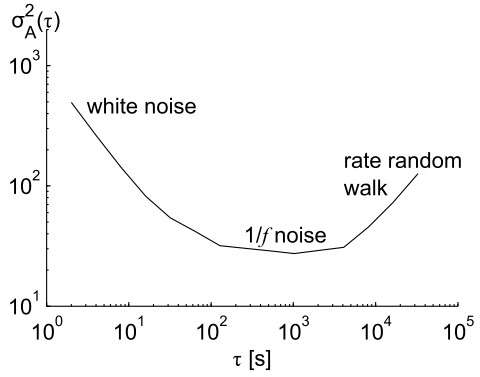

Fig. 2 An example Allan variance plot.

value of the descending white noise slope at $\tau = 1$ s. The minimum value of the Allan variance between the white noise and rate random walk slopes corresponds to the square of the bias instability of the sensor; this value is directly related to the power of $1/f$ noise [64].

2.1.3 Modeling the Measurement Errors

A key to estimating and compensating for inertial sensor measurement errors is an accurate model of the evolution of the different error components with time. Some of the most commonly encountered models of sensor error time series $x(t)$ are

- *random constant*
$$x(t) = x(t-1); \tag{2}$$
- *first-order Gauss–Markov* (GM) models of the form [9]
$$x(t) = \mathrm{e}^{-\Delta t/\gamma} x(t-1) + \eta(t) \tag{3}$$
where Δt is the time interval between steps, γ is the *correlation time* of the process, and $\eta(i)$ are independent zero-mean Gaussian random variables; and
- *random walk*
$$x(t) = x(t-1) + \eta(t) \tag{4}$$
where the random increments $\eta(i)$ are independent and zero-mean (but not necessarily Gaussian).

These three models are closely related. It can be seen that when the correlation time γ tends to infinity, GM approaches the random walk process. On the other hand, with $\gamma \to 0$, GM tends to white noise. Random walk and GM processes are examples of *autoregressive* (AR) models which are more generally expressed as

$$x(t) = \sum_{i=0}^{t-1} a(i)x(i) + \eta(t) \tag{5}$$

where $a(i)$ are known coefficients and $\eta(i)$ are independent zero-mean random variables. Sometimes the noise process η is called the driving noise. Fig. 3 shows an example realization of white noise along with the random walk and GM processes ($\gamma = 300$ samples) generated using the same noise. It can be seen that the correlated processes have significantly higher values than their driving noise.

Usually, scale factor errors are quite stable over time and can be modeled as random constants[2]. In contrast, the bias of an inertial sensor can vary significantly during operation, particularly in the case of MEMS sensors. Therefore, sensor biases are often modeled as GM or random walk processes. It should be noted that they are *Markovian* processes, i.e., the value of the process at time t only depends on the state

[2] Scale factors are not exactly constant: for instance, the scale factors of MEMS sensors depend strongly on the temperature

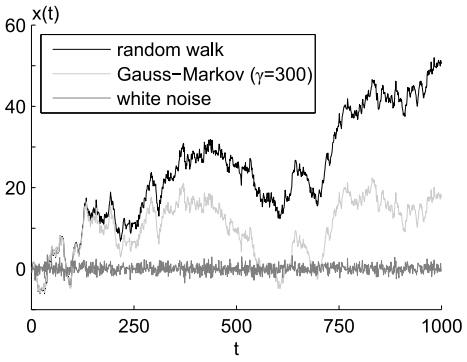

Fig. 3 Example realizations of white noise, random walk, and a first-order Gauss–Markov process

of the process at $t-1$, not on other past or future states[3]. Thus, they are suboptimal for modeling the $1/f$ bias instability process which is known to have a long memory.

It is possible to model $1/f$ processes as AR processes [35]. However, optimal modeling of a long-memory process requires an infinite number of states to be memorized [56]; for this reason, many authors have fitted finite-order AR models on sequences of data in order to predict the future behavior of, e.g., a gyroscope's bias.

2.2 Sensor Quality Grade

Inertial sensors are used for various purposes and not all use cases demand similar performance. For instance, the requirements for the gyroscope of an automotive stability control system are significantly different from the requirements for full six-degrees-of-freedom inertial navigation. Traditionally, inertial sensors have been categorized into several grades based on their performance.

Navigation grade sensors are targeted for long-term autonomous navigation whereas *tactical grade* systems are manufactured for shorter intervals of navigation, usually a few minutes. Typically, the required performance for a navigation-grade system can be that the position error must not increase by more than one nautical mile (1.85 km) after one hour of autonomous inertial navigation. For instance, navigation grade sensors can be needed for navigation systems in aircraft while a tactical grade unit can be sufficient for a missile. For examples of navigation grade IMUs, see, e.g., [27, 31]; examples of tactical grade IMUs include [46, 26].

Consumer or *automotive* grade sensors are not capable of autonomous navigation, but can be used for positioning temporarily, e.g., when satellite based positioning is not available, such as when driving through an underpass. Consumer grade

[3] There exist higher-order Gauss–Markov process where the difference equation (3) contains older values of the process

sensors, e.g., [59, 17], are primarily installed for other purposes than navigation; examples of applications are given in Section 1.3.

Table 1 Indicative specifications for IMUs of different quality grades.

Component	Parameter	Unit	Navigation	Tactical	Consumer
Accelerometer	Pre-calibration bias	mg	0.03	1	30
	Noise density	$\mu g/\sqrt{\text{Hz}}$	10	50	100
	Scale factor error	%	0.01	0.03	1
	Misalignment	mrad	0.05	0.5	–
	Cross-axis sensitivity	%	–	–	1
Gyroscope	Pre-calibration bias	°/h	0.005	1	1 000
	Bias instability	°/h	0.003	0.1	20
	Angular random walk	$^\circ/\sqrt{\text{h}}$	0.002	0.1	0.5
	Scale factor error	%	0.0005	0.01	1
	Misalignment	mrad	0.01	0.5	–
	Cross-axis sensitivity	%	–	–	1
IMU assembly[a]	Weight	kg	5	1	0.01
	Volume	cm^3	1500	500	0.01
	Power consumption	W	10	5	0.01

[a] The figures given for MEMS IMUs correspond to the sensor chip only.

Table 1 shows example specifications of different grades of inertial measurement units (IMUs); the values should be regarded as indicative orders of magnitude corresponding to the example devices referenced above, and should not be used as a definition of the different quality levels. Anyway, it is clear that the gap between consumer and navigation grades is large – the differences are in the order of many decades. Misalignment errors have not been specified for consumer-grade units because it is difficult, if not impossible, to separate their misalignment errors from other cross-coupling effects such as inter-channel electromagnetic interference; hence, the total cross-axis sensitivity is given for these IMUs instead. The consumer-grade performance figures represent low-cost bulk-manufactured MEMS sensors that are not individually calibrated by the manufacturer. When considering the size and power consumption of such a MEMS IMU, one needs to account for other necessary components such as the circuit board and readout electronics in addition to the sensor chip itself; these are not included in the example figures given for a consumer-grade IMU in Table 1. Nevertheless, it is not challenging to build a MEMS IMU into a package with size in the order of a few cubic centimeters.

When considering the performance parameters and requirements of sensors, it is important to distinguish between errors before calibration and residual errors [55]. For instance, the large bias of a consumer gyroscope can be mostly compensated for by frequent calibration (e.g., whenever the IMU is stationary), but the bias instability ultimately determines the attainable performance. On the other hand, with high-quality IMUs it may be possible to calibrate out misalignment errors to an accuracy better than the physically achievable sensor alignment precision.

3 Pedestrian Dead Reckoning

The term *dead reckoning* (DR) refers to the method where a new position estimate is computed by adding measured or estimated displacements to the coordinates of a known starting point. Inertial sensors are well known devices for providing the information on the direction and the distance traveled.

In inertial navigation, the data from three accelerometers and three gyroscopes are used to update position estimates. As described in Section 1.3.1, position estimation with INS involves the integration of gyroscope measurements to keep track of the attitude of the sensor unit, followed by double integration of acceleration measurements to obtain the velocity and position. The process of maintaining the attitude estimate and integrating the accelerations is called the strapdown INS mechanization. In this section, we will shortly discuss about the INS mechanisation and its challenges. This is followed by the detailed description of Pedestrian Dead Reckoning (PDR) and its accuracy analysis.

3.1 INS Mechanization

The traditional Inertial Navigation System (INS) mechanization includes the following tasks [60]:

1. Integration of the outputs of gyros to obtain the attitude of the system in the desired coordinate reference frame
2. Using the obtained attitude of the system, transformation of the specific force measurements to the chosen reference frame
3. Computing the local gravity in the chosen reference frame and adding it to the specific force to obtain the device acceleration in space
4. If required by the chosen reference frame, the Coriolis correction is applied
5. Double-integration of the acceleration to obtain the velocity and the position of the device

For the first task, parameterization for rotations in three-dimensional space is required. The ones selected in here are are direction cosine matrix $\mathrm{C}_{\mathrm{A}_2}^{\mathrm{A}_1}$ and rotation vector $\mathbf{p}$ with notation from [54]. Many other attitude parameterizations can be used [45]. For example, identical presentation would be possible by switching direction cosine matrices to quaternions. A 3×3 direction cosine matrix transforms a 3×1 vector from reference frame A_2 to frame A_1

$$\mathrm{C}_{\mathrm{A}_2}^{\mathrm{A}_1}\mathbf{v}^{\mathrm{A}_2} = \mathbf{v}^{\mathrm{A}_1} \tag{6}$$

The rotation vector $\mathbf{p}$ defines an axis of rotation and its magnitude defines an angle to be rotated. Similarly as direction cosine matrix, rotation vector can be used to define attitude between frames A_2 and A_1. If frame A_1 is rotated about the rotation vector $\mathbf{p}$ through the angle $p = \sqrt{\mathbf{p}^T\mathbf{p}}$ the new attitude can be uniquely used to define

frame A_2. Conversely, for arbitrary frames A_2 and A_1 we can find rotation vector that defines the relative attitude, although not uniquely. The relationship between direction cosine matrix and rotation vector is [5]

$$C_{A_2}^{A_1}(\mathbf{p}) = \begin{cases} I + \frac{\sin(p)}{p}(\mathbf{p}\times) + \frac{1-\cos(p)}{p^2}(\mathbf{p}\times)(\mathbf{p}\times) & \text{if } p \neq 0 \\ I & \text{otherwise} \end{cases} \tag{7}$$

and this can be used to transform any rotation vector to uniquely defined direction cosine matrix. In Eq. 7 $(\mathbf{p}\times)$ denotes 3×3 skew symmetric form of 3×1 vector $\mathbf{p}$.

In inertial navigation the orientation estimation beings with finding an initial orientation $A_{t=0}$ of the sensor unit with respect to some locally level frame L. Then gyro triad measurements $\omega_{IA_t}^{A_t}$ which satisfy

$$\dot{C}_{A_t}^{A_0} = C_{A_t}^{A_0}(\omega_{IA_t}^{A_t}\times) \tag{8}$$

can be used to update the orientation. In Eq. 8 I refers to inertial (non-accelerating, non-rotating) reference frame. With sufficiently short time update interval dt an approximation $\mathbf{p}_t \approx \omega_{IA_t}^{A_t} dt$ can be used and then Task 1 is completed by updating $C_{A_t}^{L}$ at each computer cycle:

$$C_{A_t}^{L} \leftarrow C_{A_{t-1}}^{L} C_{A_t}^{A_{t-1}}(\mathbf{p}_t) \tag{9}$$

In Task 2 the accelerometer triad measurement

$$\mathbf{a}_{SF}^{A_t} = \ddot{\mathbf{r}}^{A_t} - \mathbf{g}^{A_t}, \tag{10}$$

is transformed to L frame using Eq. 9, which leads to differential equation for position to be solved

$$\ddot{\mathbf{r}}^{L} = C_{A_t}^{L}\mathbf{a}_{SF}^{A_t} + \mathbf{g}^{L}, \tag{11}$$

where $\mathbf{g}^{L}$ is result from Task 3. Solving Eq. 11 completes Task 5. In this compact introduction the Task 4 was neglected in Eq. 9. In the double-integration of accelerations even a small error in acceleration measurement yields a large position error drift in the output. Because the accelerometers measure the specific force instead of the true acceleration of the sensor unit, as explained in Section 1.1, the gravitational acceleration is added to the vertical acceleration component; this is straightforward when the accelerations are first transformed to a local level frame (Eq. 11). However, because the gravity compensation of accelerations require the coordinate transformation, any error in gyroscope output causes errors in the transformed accelerations, which in turn introduces increasing errors to the computed accelerations through the errors in the gravity compensation. As the gyro outputs are integrated to form the coordinate transformation and the transformed accelerations are double-integrated for position estimate, the gyro errors produce a position error which increases with time cubed. Therefore the gyro performance is very critical in INS implementations. Effect of gyro errors can be reduced with GNSS integration but this is quite difficult with consumer-grade sensors due to linearization problems [42].

As the requirements for sensor accuracies are very strict for the strapdown INS mechanization, requiring very high-quality and expensive sensor units, the developers of mass-market applications are looking for solutions where multiple integrations of sensor errors can be avoided. In pedestrian applications, the cyclic nature of the human gait can be utilized to enable navigation with low-cost inertial sensors. Two approaches have become popular in the literature: mounting the sensors to the user's shoe and evaluating the INS mechanization equations in a stepwise manner; and Pedestrian Dead Reckoning (PDR) where the position estimate is propagated by detecting steps and estimating their length, and keeping track of the heading using body-mounted sensors.

The concept of foot-mounted inertial navigation hinges on the idea that when the sensor unit is known to be stationary, the velocity errors can be observed [19]; this condition holds regularly for a pedestrian's foot when walking. In addition to resetting velocity this allows to estimate and compensate for other errors that are correlated with the velocity errors, e.g. position and attitude offsets and sensor biases. The most important benefit of foot-mounted inertial navigation is the fact that it is insensitive to the direction of the step and gait characteristics as long as the foot stance periods can be properly detected. However, detecting the stance phase is not trivial especially when the user is running or moving in stairs [57, 50]. In addition, the foot is subject to higher dynamics than the rest of the body; the sensors are subject to a significant shock whenever the foot hits the ground, which can lead to temporary measurement errors.

In PDR, instead of double-integration of the accelerations, the speed of the walk is estimated from the periodical acceleration waveform produced by pedestrian movements. The speed can be estimated either from the main frequency of the periodic signal or by detecting individual steps and estimating their lengths and durations from the acceleration waveform. This information along with estimated heading is used to propagate the estimate of user position. It can be shown that PDR mechanization is superior to the traditional INS mechanization for a person on foot when the sensors are mounted on the user's torso [44]. The main drawback of PDR is the limitation to one motion mode; the mechanization works only when walking while the general strapdown INS mechanization works without any assumptions about the user motion. In addition, while foot-mounted inertial navigation is 3-dimensional by nature, PDR is 2-dimensional and requires height information from other sources such as map [66] or barometric altimeter.

3.2 Step Detection with Accelerometers

In this section step detection with torso mounted sensors are considered in detail. With *step* we mean the displacement of one foot during walking movement, i.e. the distance between two consecutive foot prints. The occurrence of a step can be easily detected from the signal pattern of the vertical acceleration component [40]. However, this approach is sensitive to orientation errors of the sensor unit, as it is as-

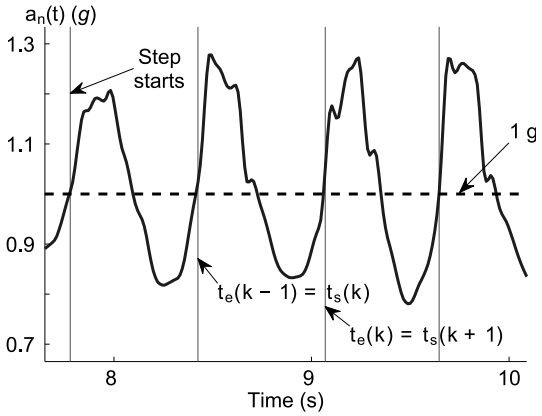

Fig. 4 Detection of steps from acceleration norm.

sumed that one axis is aligned with vertical or that the transformation to the vertical is known. Other possibility it to compute the magnitude of the measured acceleration vector, i.e. the norm of acceleration [33]. Most commonly the step detection is based on accelerometers but also gyroscopes can be used [14]. The signal pattern varies according to where the user attaches the sensor unit [38]. Typical choices to wear the sensor unit are on the belt, e.g. on the side of the user or on lower back, or onto upper parts of the torso, e.g. attach it to the shoulder strap of a backpack or wear it in a chest pocket. Step detection is often based on the detection of signal peaks [38] or crossings of the signal with its average [33] or some other reference level [43]. Often the detection algorithm combines both peak detection and detection of reference level crossings. For example, step detection from acceleration norm may consists of the following steps:

1. Low pass filtering and resampling the signal; sampling frequency in the range 20–25 Hz is high enough.
2. Computation of the norm of current acceleration sample, i.e.,

$$a_n(t) = \sqrt{a_x^2(t) + a_y^2(t) + a_z^2(t)}, \tag{12}$$

   where $a_n(t)$ is the acceleration norm and $a_x(t)$, $a_y(t)$, and $a_z(t)$ are the filtered components of the measured acceleration.
3. Instances of step starts $t_s(k)$ are detected by observing the g-crossings of the acceleration norm that are followed by a rise rate and a peak height that exceed the preset limits, and requiring that the time between the current and previous g-crossings is long enough.
4. The step end $t_e(k)$ is considered to be found when the next step starts or when a predefined time, considered as the maximum duration of one step, has passed after the start of the current step.

An example with acceleration norm and the detected step starts is shown in Fig. 4. The data for the figure were recorded using a sensor unit that was attached to the

belt and positioned to the back of the test walker. Other methods that can be used to detect individual steps include the correlating of sensor signal with predefined stride template [7]. The template is formed offline, e.g., by recording it from sample walk [25]. The correlation method can be improved by using dynamic time warping (DTW) which allows non-linear mapping between the template and the online signal [52].

There are applications and devices, such as mobile phones, where the orientation of the sensor unit cannot be assumed to be predetermined and constant. If the methods for step detection and step length estimation require e.g. vertical acceleration component, the phone orientation need to be tracked or the motion classification can be used to allow adapting different algorithms for different motion modes [13].

3.3 Step Length Estimation

There are two main categories for methods to estimate step length. The first category includes models that are based on the biomechanical principles whereas the models in the second category are based on empirical relationships between acceleration signal pattern and step length. With biomechanical models, certain user-related parameters, such as leg length, are needed in addition to the empirically determined scaling parameters [32]. In empirical models, the acceleration norm $a_n(t)$ or the vertical acceleration component $a_v(t)$ are typically used for step length estimation. The signal patterns that have been found to correlate well with step length include the following:

$$\text{Main frequency} \quad p_1(k) = 1/(t_e(k) - t_s(k)) \tag{13}$$

$$\text{Variance, } a_n \quad p_2(k) = \text{var}(a_n(t)), \quad t_s(k) \le t < t_e(k) \tag{14}$$

$$\text{Variance, } a_v \quad p_3(k) = \text{var}(a_v(t)), \quad t_s(k) \le t < t_e(k) \tag{15}$$

$$\text{Area integral} \quad p_4(k) = \int_{t_s(k)}^{t_e(k)} |a_n(t) - g|\, dt \tag{16}$$

$$\text{Maximum difference, } a_n \quad p_5(k) = \max a_n(t) - \min a_n(t), \quad t_s(k) \le t < t_e(k) \tag{17}$$

$$\text{Maximum difference, } a_v \quad p_6(k) = \max a_v(t) - \min a_v(t), \quad t_s(k) \le t < t_e(k) \tag{18}$$

Instead of (13), the main frequency of the periodical signal can be obtained using Fast Fourier Transformation (FFT) [40, 38]. In (14)-(15) the variance of the acceleration signal (e.g., norm or vertical component) is computed over a time window comparable to some step durations [38], e.g. over one step. The area integral (16) is obtained by integrating over one step duration the absolute value of the acceleration norm where the local gravity has been subtracted [33]. In (17)-(18) the difference

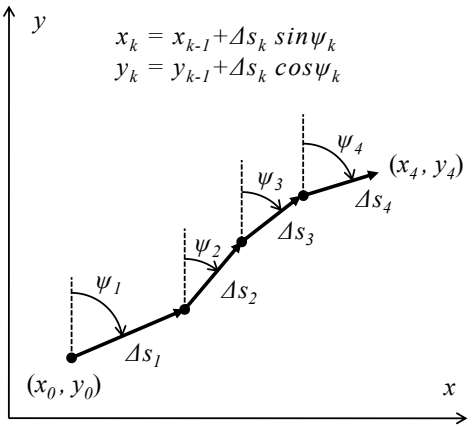

Fig. 5 Dead reckoning in two dimensions.

between the maximum and minimum acceleration (e.g., norm or vertical component) of a detected step is used [32].

Also the use of combinations of these signal patterns has been proposed [38, 32], as well as slightly different patterns from these [43]. The empirical step length model often includes at least one empirically determined parameter. In many cases a non-linear function, such as raising to a power or extraction of root, has to be applied to the signal pattern. It is also common to add constant offsets to the pattern or the function [38, 23]. A generic form of the step length model can be written as

$$\Delta s_k = K_{j.q}\, p_j(k)^q + b \tag{19}$$

where Δs_k is the distance traveled and $p_j(k)$ is the signal pattern, both computed for the k^{th} step. $K_{j.q}$ is the scaling factor, b is the offset, and q is the exponent that defines the function to be applied on p_j. The performance of step length estimation with different functions applied on different signal patterns were demonstrated with real pedestrian data in [11]. With the best combinations, the relative error in the estimated distance traveled was 2–3 %.

The step length models discussed here are applicable in flat floor or terrain. In stairs, the step length is forced to be shorter. A method based on analysis of accelerometer and gyro signal patterns can be used to detect forward direction and going up or down in stairs [36].

3.4 PDR Mechanization

In PDR mechanization, the dead reckoning process involves step detection and step length estimation, as shown in the diagram of Fig. 6. The PDR position estimate is

computed by starting from initial coordinates, x_0, y_0, and initial heading angle ψ_0. As the DR method is not able to determine absolute positions, these initial estimates have to determined using alternative positioning methods, such as radio navigation or satellite based positioning.

While the position in PDR algorithm is updated only when step ends are detected, the heading is updated every Δt_g seconds, i.e., at the sampling frequency of the gyro:

$$\psi_\lambda = \psi_{\lambda-1} + \omega_\lambda \Delta t_g, \tag{20}$$

where ω_λ is the angular rate measurement by the gyro at the sampling instance $\lambda \Delta t_g$. In position estimation, a heading estimate representative of the whole step duration is needed. Therefore the heading is averaged over the step duration:

$$\bar{\psi}_k = \frac{1}{n_k} \sum_{\lambda \in \Lambda_k} \psi_\lambda, \qquad \Lambda_k = \left\{ \lambda : \lambda \text{ is an integer}, \frac{t_s(k)}{\Delta t_g} \leq \lambda < \frac{t_e(k)}{\Delta t_g} \right\}, \tag{21}$$

where n_k is the number of samples in Λ_k. The heading and horizontal coordinates are propagated by

$$\begin{aligned} x_k &= x_{k-1} + \Delta s_k \cos \bar{\psi}_k \\ y_k &= y_{k-1} + \Delta s_k \sin \bar{\psi}_k, \end{aligned} \tag{22}$$

where Δs_k is the estimated step length, i.e., the distance traveled during the step with index k. Position estimates that are based on step detection and step length estimation are available at step intervals Δt_k, which vary according to the walking style and the speed of the pedestrian.

The orientation of the sensor unit with respect to the direction of pedestrian travel is not fixed in smart phones and many other mobile devices. To determine the step direction, the knowledge about the orientation of the device with respect to the environment is required but it is not enough [36, 13]. Methods to estimate the unknown alignment between the mobile device and the pedestrian (and the step direction) are compared in [12].

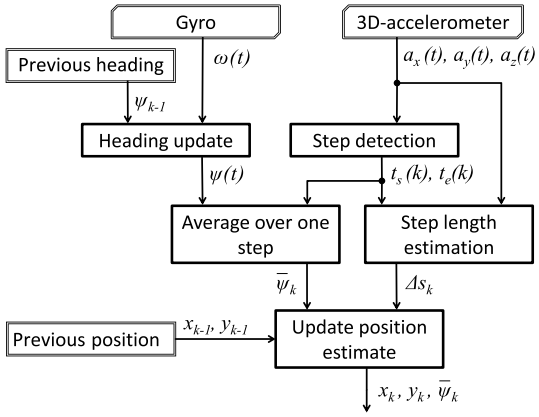

Fig. 6 Block diagram of the PDR algorithm.

Table 2 Effect of 1% scale factor error in accelerometer to functions of signal patterns for step length estimation.

Function	Raw $p_j(k)$	Square root $p_j(k)^{1/2}$	Cube root $p_j(k)^{1/3}$	Fourth root $p_j(k)^{1/4}$
Step length error (%)	1.00	0.50	0.33	0.25

Effect of Sensor Quality Grade to the Accuracy of PDR

Although PDR mechanization is not as sensitive to sensor errors as the traditional INS mechanization, the grade of sensors still has an effect to the performance of the PDR. In this section, the accumulation of errors in PDR is studied based on simple test cases.

From (13)–(18) it can be seen that the step length estimate is not sensitive to accelerometer bias: in p_2, p_3, p_5, and p_6 the bias is totally canceled out and in p_1 and p_4 its effect is small. Contrary to the bias error, the effect of the scale factor error on all other signal patterns except p_1 is directly proportional to the sensor error. However, taking square root, cube root or the fourth root of the signal pattern decreases the effect of accelerometer scale factor error on the step length estimate, as can be seen in Table 2.

If the scale factor error of the accelerometer is constant, its effect can be taken into account in the scaling factor of the step length model (19). In practice the scale factor error of a consumer grade accelerometer based on MEMS technology is slowly changing as a function of internal conditions of the sensing element, such as the temperature. If the temperature effect on the sensor scale factor at its maximum is 1%, then the effect on the estimated distance traveled is the same as the relative error of the evaluated function (Table 2) at the most. These values are small when compared with step length modeling errors reported in literature [32, 11].

The effect of the gyro quality to PDR estimates can be analyzed by the simulation of a PDR system defined by (20)–(22). The effect of the gyro bias is simulated by using a scenario where the pedestrian walks with constant step length of 0.75 m and constant frequency of 2 steps/s along the positive x-axis. The gyro bias is assumed

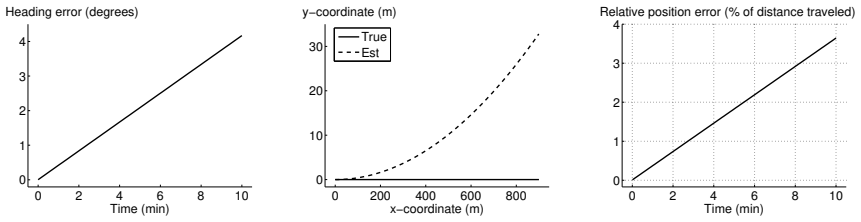

(**a**) (**b**) (**c**)

Fig. 7 Effect of 25°/h gyro bias when the pedestrian is walking with constant speed along the positive x-axis: (**a**) heading error; (**b**) true and estimated coordinates; (**c**) relative position error

Table 3 Comparison of gyro grade with respect to the effect of uncompensated bias to the PDR error build-up.

	Navigation	Tactical	Consumer
Bias instability ($^\circ$/h)	0.0035	1	25
Time to 2% relative position error	27 days	2.3 h	5.5 min
Time to 3% relative position error	41 days	3.4 h	8.3 min
Time to 3° heading error	35 days	3.0 h	7.2 min

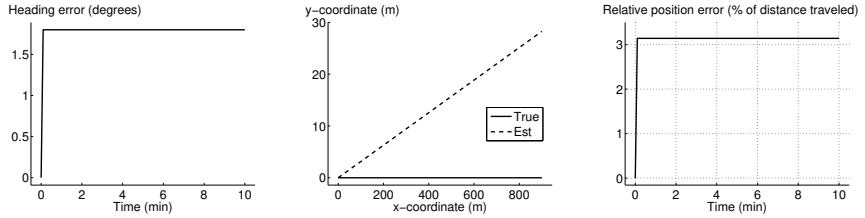

(**a**) (**b**) (**c**)

Fig. 8 Effect of 1% gyro scale factor error when the pedestrian has made a 180° turn from -180° and then walks with constant speed along positive x-axis: (**a**) heading error; (**b**) true and estimated coordinates; (**c**) relative position error

to be 25°/h, which is a typical bias instability of consumer grade gyros (Table 1). The development of heading error, error in estimated position and the position error relative to the distance traveled is shown in Fig. 7. The heading error grows linearly (Fig. 7a), the error in the y-coordinate grows quadratically[4] with respect to the x-coordinate and time (Fig. 7b), and the relative position error with respect to the distance traveled grows almost linearly (Fig. 7c). With the best step length models, the long term average in the relative positioning error is about 2–3% [11]. With the given simulation parameters, the relative positioning error introduced by the gyro bias is smaller in the beginning, but exceeds 2% in less than 6 minutes and 3% in less than 9 minutes.

To compare the gyro grades described in Table 1, the simulations were also run with gyro instabilities typical to navigation and tactical grade gyros. The results are shown in Table 3.

The effect of the gyro scale factor error is simulated by using a scenario where the pedestrian first makes a 180° turn and then walks with a constant step length of 0.75 m and a constant frequency of 2 steps/s along the positive x-axis. The gyro scale factor error is assumed to be 1%, which corresponds to the scale factor uncertainty due to the temperature sensitivity over 50 K in a consumer grade gyro [6]. The heading error, the error in the estimated position, and the position error relative to the distance traveled are shown in Fig. 8. In this simulation, the heading error grows in the turn to 1.8° and then stays constant, as the scale factor error has an ef-

[4] The growth is almost quadratic with small heading errors; however, with larger heading errors, the sine and cosine functions in (22) bound the error growth.

fect only when the gyro senses a non-zero anular rate (Fig. 8a). Due to the constant heading error, the position error grows linearly with respect of time and x-coordinate (Fig. 8b). In the initial turn, the position error relative to the distance traveled jumps directly to more than 3% (Fig. 8c). That is, whith the parameters used in this simulation and after a 180° turn, the error due to the gyro scale factor error is larger than the error introduced by the best step length models in [11].

To compare the gyro grades described in Table 1, the simulations were also run with gyro scale factor errors typical to navigation and tactical grade gyros. The results are shown in Table 4.

Table 4 Comparison of gyro grade with respect to the effect of uncompensated scale factor error to the PDR error build-up.

	Navigation	Tactical	Consumer
Scale factor error (%)	0.001	0.015	1
Constant heading error (degrees)	0.0018	0.027	1.8
Constant relative position error (%)	0.00314	0.047	3.14

It should be noted that the simulation results given in this section apply only on PDR mechanization of inertial sensors. The growth of position error is much faster with traditional INS mechanization, partly due to the low speed of the pedestrian and partly due to the algorithm simplifications allowed by the characteristics of pedestrian movements. Another important remark considers the effect of the tilt error of the heading gyro: the simulations assume that the sensitive axis of the gyro is aligned with vertical. However, in practice the sensor unit easily gets tilted by a couple of degrees, which introduces a scaling error to the gyro output.

4 Infering Context with Inertial Sensors

In addition to providing data for navigation purposes, inertial sensors can be used to increase the context awareness of a device. One widely used application is motion mode classification. In Fig. 9 the waveform of the norm of accelerometer measurements, as defined in Eq. (12), is shown. The different characteristics in waveform depending on motion mode is clearly seen. When walking, foot impacts clearly increase the variability of the signal. When driving a car, engine vibrations, vehicle accelerations, and road imperfections cause variations which are smaller than those occurring during walking. Yet, these variations are distinguishable from the case of a stationary device where the only source of variation is measurement noise.

In order to have a computer to identify these motion modes, features such as sample variance or peak frequency need to be extracted from the acceleration data. Fig. 10 shows two such features: the sample standard deviation σ and the peak frequency from non-overlapping five-second windows. In this example, the classifi-

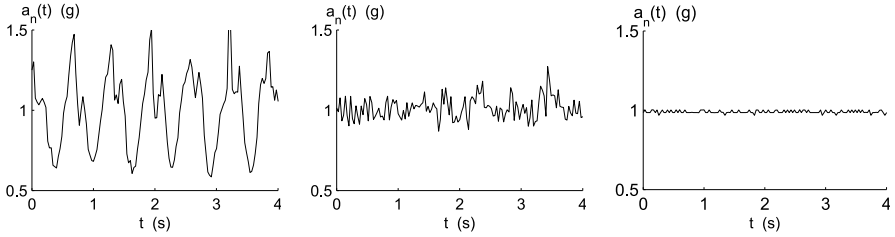

Fig. 9 Norm of accelerometer output in different motion modes: (**a**) walking, $\sigma = 0.24\,g$; (**b**) driving, $\sigma = 0.071\,g$; (**c**) stationary, $\sigma = 0.0084\,g$

cation is relatively easy, as the characteristics are clearly distinguishable and there is only one label to learn. In practice, the classification problems are more complex, with overlapping features and multiple labels [69]. Thus, proper algorithms and statistical tools are needed to obtain useful classification results. In this section a brief introduction to such tools is given.

4.1 Pattern Recognition

As a simplified statistical example, pattern recognition problem can be considered as discrimination between r multivariate normal populations. The Bayes theorem is applied to obtain the probability of the originating population class (e.g. motion mode) given the statistics (e.g. features) obtained from the sensor data.A training data set with labeled motion modes is needed to obtain the class means μ_j and covariances Σ_j for each class j. Then, according to the model, the future observations collated to a q-dimensional feature vector $\mathbf{z}$ are distributed as

$$\mathbf{z}_j \sim N(\mu_j, \Sigma_j). \tag{23}$$

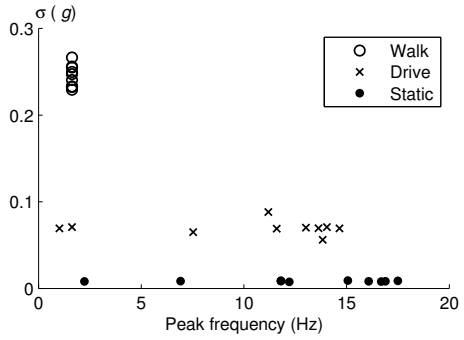

Fig. 10 Standard deviation and peak frequency as features

It should be stressed that due to limited size of the training data set the mean vector $\mu_j \in \mathbb{R}^q$ and the covariance matrix $\Sigma_j \in \mathbb{R}^{q \times q}$ are actually estimates of the true model parameters. Further simplification is made by assuming that the the prior probability $P(C = j)$, where $C = j$ denotes an event that the correct class is j is known. Under these assumptions, Bayes' theorem can be applied to obtain

$$P(C = j|\mathbf{z}) = \frac{p_{\mathbf{z}_j} P(C = j)}{p_{\mathbf{z}}}, \tag{24}$$

where

$$p_{\mathbf{z}} = \sum_{i=1}^{r} p_{\mathbf{z}_i} P(C = i). \tag{25}$$

The actual classification result is obtained by finding the class that maximizes the posterior probability $P(C = j|\mathbf{z})$. Adding inference for sequential data can be done, for example, using Markov model for state transition probabilities $P(C_t = h)|P(C_{t-1} = k)$ for all possible states $h,k = 1,\ldots,r$. In practice, the assumption that distributions and correlations between features are known is often invalid as the feature set may include binary features, multimodally distributed features and Wishart distributed features (due to sampling in training phase). Thus, in modern machine learning more generalizable and scalable methods, such as gradient tree boosting are popular [10]. Even though the new methods in machine learning require less assumptions for the inputs, there is still a need to understand what kind of data and features should be included. When inertial sensors are used for classification there are many options for feature engineering if the basic principles of inertial sensors are understood well. Features can be extracted from raw data (angular rates, specific force) or from integrated data (position, velocity, orientation). When characteristics of sensor noise are identified the effectiveness of high frequency versus low frequency features may become apparent. Such examples of advanced features are given in the following section.

4.2 Feature Extraction

Two very important features for classification of motion modes shown in Fig. 10 were examples of statistical (variance) and frequency domain (peak frequency) features. Using windowed raw sensor data there are many other features easily obtainable such as [16]:

- Skewness
- Mean absolute deviation
- Zero-crossing rate
- Sub band energies and their ratios
- Change in the peak frequency over 4 sub-frames
- Frequency domain entropy

To make the classification more efficient, there exist efficient algorithms that can be used reduce the dimensionality of feature space by utilizing the correlation between features [65].

To show how knowledge of inertial navigation theory may help in classification the effect known as coning is introduced. The relation between gyroscope measurements and device orientation with fast processing rate was shown in Eqs. (7,9). However, the exact relation between rotation vector and gyroscope measurements is [5]

$$\dot{\mathbf{p}} = \omega_{\mathrm{IA_t}}^{\mathrm{A_t}} + \frac{1}{2}\mathbf{p} \times \omega_{\mathrm{IA_t}}^{\mathrm{A_t}} + \frac{1}{p^2}(1 - \frac{p\sin(p)}{2(1-\cos(p))})\mathbf{p} \times (\mathbf{p} \times \omega_{\mathrm{IA_t}}^{\mathrm{A_t}}) \tag{26}$$

and the last two terms, describing non-commutativity rate, begin to play a role if the attitude update rate is too slow. Important feature in this equation is that the cross product terms remain zero if gyro signal vector ($\omega_{\mathrm{IA_t}}^{\mathrm{A_t}}$) keeps its direction. If the gyro signal is constant or the object can rotate only about one fixed axis, then there is no problem of non-commutativity. The problem arises if gyro data is averaged, assuming

$$\dot{\mathbf{p}} \approx \omega_{\mathrm{IA_t}}^{\mathrm{A_t}} \tag{27}$$

and the true rotation is lost due to non-commutativity of rotations. Typically in inertial sensor processing this is avoided by performing the direction cosine update with fast rate with respect to motion (or applying coning correction terms). In this context we loosely define the error due to approximation in Eq. 27 as coning motion. To see why this is important in motion classification, consider following scenarios for time period $n \rightarrow m$

- Unit is in smartwatch attached to wrist of a pedestrian
- Unit is fixed to a vehicle that is cornering
- Unit is stationary on table, gyros have constant bias

Gyroscope data samples at 20 Hz from these scenarios is shown in Fig. 11. To see the effect of coning errors, this data is resampled by averaging to 1 Hz and maximum angle error with respect to 20 Hz reference is plotted in Fig. 12. By combining amount of coning error in each case we will see that first example has quite large non-commutativity rate, vehicular motion clearly less and the in the static case the coning error is negligible. The coning effect computed this way is a direct measure of complexity of angular motion experienced, and thus an useful, acceleration independent feature for motion mode classification. It may also help obtaining more insight on how the user experiences the motion [61]. It should be noted that orientation with fast rate is already computed by the inertial processing algorithm, so the only extra work for deriving this feature is to take direct average of gyro data, multiply it by time interval and apply it in Eq. 7 ($\mathbf{p} \leftarrow \frac{n-m}{N}\sum\omega$). Extension this method to specific coning correction algorithms [30] and accelerometer processing (velocity rotation compensation) is also straightforward. This illustrates the importance of feature engineering in machine learning, to build effective feature it is important to know what the sensors actually measure.

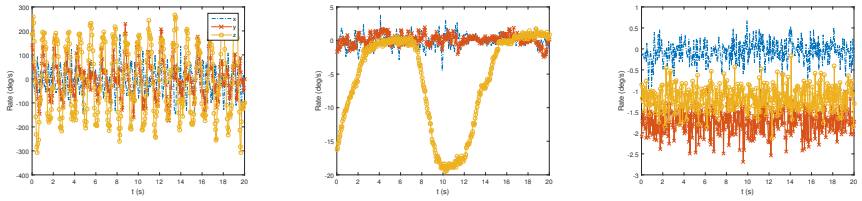

(**a**) (**b**) (**c**)

Fig. 11 Gyro data in different cases: (**a**) Smartwatch; (**b**) Driving; (**c**) Biased, stationary. Note the y-axis scales

Combination of bias and moderate non-coning motion (such as in vehicle mode) may also result in large coning error. This is because direction of apparent rotation vector is changing when another component changes its magnitude. Thus the motion mode recognition and orientation estimation are not necessarily independent tasks. The quality of sensors affects input features, but on the other hand, known motion mode can be used to infer gyroscope biased, for example.

4.3 Classification Accuracy

In practice it is impossible to implement a classifier that makes no mistakes; misclassifications will occur from time to time. From the viewpoint of the application designer, the classification accuracy can be evaluated for two different cases: (a) the expected misclassification rate prior to observing the features, and (b) the probability of misclassification given the observed feature vector. For the former, the overlap in the training data is a good indicator. For the latter, (24) directly gives such probability, but as mentioned the multinormal model for features is rarely valid. Often the system designer has no other choice than to collect sufficient amount of independent data for cross-validation to obtain realistic values for misclassification rates. In addition, one approach to tolerate misclassification is to apply partial classifica-

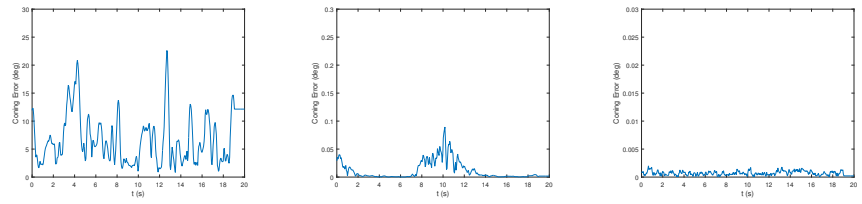

(**a**) (**b**) (**c**)

Fig. 12 Coning error in degrees in the three cases: (**a**) Smartwatch; (**b**) Driving; (**c**) Biased, stationary. Note the y-axis scales

tion methods, where the option of not classifying a situation at all is reserved [8]. In motion mode classification the number of classes can vary a lot, which affects the classification accuracy, but generally the reported mis-classification error rate is almost always below 10 % [16].

4.4 Areas of Application

Motion mode using sensors in smartphones is already generally available [21] and applications are growing in number continuously. For example, detailed motion mode information would be valuable for remote monitoring of elderly people [62]. The modern machine learning tools such as XGBoost seems to be very effective in this this [63]. For navigation applications the detection of Walking-mode allows using PDR, and many other context-dependent mechanizations or filter profiles have been proposed [15]. The sequential nature of navigation problem has to be taken into account in recognition [49, 16]. In principle, motion mode classification methods can be used in any area where human motion is involved and the subjects exhibit distinct signatures [3]. The list of available applications is not limited to human motion mode, as the market for Internet of Things devices is growing in the industrial side as well and general tendency is to include inertial sensors in all kinds devices that are experiencing motion, without forgetting the increasing amount of smartphone applications [68].

5 Summary

With the development of low-cost MEMS accelerometers and gyroscopes, more and more motion-aware applications become achievable. Since inertial sensors measure motion parameters the input is based on physical properties specific to the application; emerging applications are usually significantly different from the original use of inertial sensors, i.e., navigation. Novel applications typically are less strict in sensor accuracy requirements than traditional inertial navigation systems. However, imprecision may cause the application to perform poorly in certain situations. Common methods to improve the performance is to calibrate the inertial sensors and to filter the sensor data appropriately. Understanding of physical principles of inertial sensor measurements is essential in designing systems that involve motion measurement. In this chapter, an introduction to inertial sensor applications was provided. Such a concise presentation did not permit in-depth treatment of inertial navigation system algorithms and other applications. More information about these topics and future trends can be found, e.g., in [60, 22, 13, 16, 48, 58].

References

1. Aguiar, B., Rocha, T., Silva, J., Sousa, I.: Accelerometer-based fall detection for smartphones. In: Medical Measurements and Applications (MeMeA), 2014 IEEE International Symposium on, pp. 1–6. IEEE (2014)
2. Allan, D.W.: Statistics of atomic frequency standards. Proc. IEEE **54**(2), 221–230 (1966)
3. Altun, K., Barshan, B., Tunçel, O.: Comparative study on classifying human activities with miniature inertial and magnetic sensors. Pattern Recogn. **43**, 3605–3620 (2010)
4. Armenise, M.N., Ciminelli, C., Dell'Olio, F., Passaro, V.: Advances in Gyroscope Technologies. Springer Verlag (2010)
5. Bortz, J.E.: A new mathematical formulation for strapdown inertial navigation. IEEE Transactions on Aerospace and Electronic Systems **AES-7**(1), 61–66 (1971). DOI 10.1109/TAES.1971.310252
6. Bosch Sensortec: BMI160 small, low power inertial measurement unit. rev. 08. Doc.Nr. BST-BMI160-DS000-07, Data sheet (2015)
7. Brajdic, A., Harle, R.: Walk detection and step counting on unconstrained smartphones. In: Proceedings of the 2013 ACM International Joint Conference on Pervasive and Ubiquitous Computing, UbiComp '13, pp. 225–234. ACM, New York, NY, USA (2013)
8. Broffit, J.D.: Nonparametric classification. In: P.R. Krishnaiah, L.N. Kanal (eds.) Handbook of Statistics 2. North-Holland (1990)
9. Brown, R.G., Hwang, P.Y.C.: Introduction to Random Signals and Applied Kalman Filtering, 3rd edn. John Wiley & Sons (1997)
10. Chen, T., Guestrin, C.: Xgboost: A scalable tree boosting system. In: Proceedings of the 22Nd ACM SIGKDD International Conference on Knowledge Discovery and Data Mining, KDD '16, pp. 785–794. ACM, New York, NY, USA (2016). DOI 10.1145/2939672.2939785. URL http://doi.acm.org/10.1145/2939672.2939785
11. Collin, J., Davidson, P., Kirkko-Jaakkola, M., Leppäkoski, H.: Inertial sensors and their applications. In: S.S. Bhattacharyya, E.F. Deprettere, R. Leupers, J. Takala (eds.) Handbook of Signal Processing Systems. Springer New York (2013)
12. Combettes, C., Renaudin, V.: Comparison of misalignment estimation techniques between handheld device and walking directions. In: 2015 International Conference on Indoor Positioning and Indoor Navigation (IPIN), pp. 1–8 (2015). DOI 10.1109/IPIN.2015.7346766
13. Davidson, P., Piche, R.: A survey of selected indoor positioning methods for smartphones. IEEE Communications Surveys Tutorials **PP**(99), 1–1 (2016). DOI 10.1109/COMST.2016.2637663
14. Diaz, E.M., Gonzalez, A.L.M.: Step detector and step length estimator for an inertial pocket navigation system. In: 2014 International Conference on Indoor Positioning and Indoor Navigation (IPIN), pp. 105–110 (2014)
15. Dixon, R., Bobeye, M.: Performance differentation in a tightly coupled gnss/ins solution. In: Proc. ION GNSS+ 2016 (2016)
16. Elhoushi, M., Georgy, J., Noureldin, A., Korenberg, M.J.: A survey on approaches of motion mode recognition using sensors. IEEE Transactions on Intelligent Transportation Systems (2016). DOI 10.1109/TITS.2016.2617200
17. Fairchild Semiconductor Corporation: FIS1100 6D Inertial Measurement Unit with Motion Co-Processor and Sensor Fusion Library (2016). Data sheet rev. 1.2
18. Farrell, J.: Aided navigation: GPS with high rate sensors. McGraw-Hill, Inc. (2008)
19. Foxlin, E.: Pedestrian tracking with shoe-mounted inertial sensors. IEEE Computer Graphics and Applications **25**(6), 38–46 (2005). DOI 10.1109/MCG.2005.140
20. Gianchandani, Y.B., Tabata, O., Zappe, H.P.: Comprehensive microsystems. Elsevier (2008)
21. Google: DetectedActivity API for Android. https://developers.google.com/android/reference/com/google/android/gms/location/DetectedActivity (2017). [Online; accessed 29-March-2017]
22. Groves, P.: Principles of GNSS, Inertial, and Multisensor Integrated Navigation Systems, Second Edition:. GNSS/GPS. Artech House (2013). URL https://books.google.fi/books?id=t94fAgAAQBAJ

23. Gusenbauer, D., Isert, C., Krsche, J.: Self-contained indoor positioning on off-the-shelf mobile devices. In: 2010 International Conference on Indoor Positioning and Indoor Navigation, pp. 1–9 (2010)
24. Hanning, G., Forslöw, N., Forssén, P.E., Ringaby, E., Törnqvist, D., Callmer, J.: Stabilizing cell phone video using inertial measurement sensors. In: Computer Vision Workshops (ICCV Workshops), 2011 IEEE International Conference on, pp. 1–8. IEEE (2011)
25. Harle, R.: A survey of indoor inertial positioning systems for pedestrians. IEEE Communications Surveys Tutorials **15**(3), 1281–1293 (2013)
26. Honeywell Aerospace, Phoenix, AZ, USA: HG1700 Inertial Measurement Unit (2016). Data sheet N61-1619-000-000 I 09/16
27. Honeywell Aerospace, Phoenix, AZ, USA: HG9900 Inertial Measurement Unit (2016). Data sheet N61-1638-000-000 I 10/16
28. IEEE standard for inertial sensor terminology. IEEE Std 528-2001 (2001)
29. IEEE standard specification format guide and test procedure for single-axis laser gyros. IEEE Std 647-1995 (1996)
30. Ignagni, M.: Optimal strapdown attitude integration algorithms. Journal of Guidance, Control, and Dynamics **13**(2), 363–369 (1990)
31. iMAR Navigation GmbH, St. Ingbert, Germany: iNAT-RQH400x (2017). Data sheet rev. 1.13
32. Jahn, J., Batzer, U., Seitz, J., Patino-Studencka, L., Gutiérrez Boronat, J.: Comparison and evaluation of acceleration based step length estimators for handheld devices. In: Proc. Int. Conf. on Indoor Positioning and Indoor Navigation, pp. 1–6. Zurich, Switzerland (2010)
33. Käppi, J., Syrjärinne, J., Saarinen, J.: MEMS-IMU based pedestrian navigator for handheld devices. In: Proc. ION GPS, pp. 1369–1373. Salt Lake City, UT (2001)
34. Keshner, M.S.: $1/f$ noise. Proc. IEEE **70**(3), 212–218 (1982)
35. Kirkko-Jaakkola, M., Collin, J., Takala, J.: Bias prediction for MEMS gyroscopes. IEEE Sensors J. (2012). DOI 10.1109/JSEN.2012.2185692
36. Kourogi, M., Kurata, T.: Personal positioning based on walking locomotion analysis with self-contained sensors and a wearable camera. In: The Second IEEE and ACM International Symposium on Mixed and Augmented Reality, 2003. Proceedings., pp. 103–112 (2003). DOI 10.1109/ISMAR.2003.1240693
37. Krobka, N.I.: Differential methods of identifying gyro noise structure. Gyroscopy and Navigation **2**, 126–137 (2011)
38. Ladetto, Q.: On foot navigation: continuous step calibration using both complementary recursive prediction and adaptive Kalman filtering. In: Proc. ION GPS, pp. 1735–1740. Salt Lake City, UT (2000)
39. Leland, R.P.: Mechanical-thermal noise in MEMS gyroscopes. IEEE Sensors J. **5**(3), 493–500 (2005)
40. Levi, R.W., Judd, T.: Dead reckoning navigational system using accelerometer to measure foot impacts. U.S. Patent 5,583,776 (1996)
41. Lightman, K.: Silicon gets sporty. IEEE Spectrum **53**(3), 48–56 (2016)
42. Martin, H., Groves, P., Newman, M.: The limits of in-run calibration of mems inertial sensors and sensor arrays. Navigation **63**(2), 127–143 (2016). DOI 10.1002/navi.135. URL `http://dx.doi.org/10.1002/navi.135`. Navi.135
43. Meriheinä, U.: Method and device for measuring the progress of a moving person. U.S. Patent 7,962,309 (2007)
44. Mezentsev, O., Collin, J., Lachapelle, G.: Pedestrian Dead Reckoning – A Solution to Navigation in GPS Signal Degraded Areas. Geomatica **59**(2), 175–182 (2005)
45. Nitschke, M., Knickmeyer, E.H.: Rotation parameters-a survey of techniques. Journal of surveying engineering **126**(3), 83–105 (2000)
46. Northrop Grumman LITEF GmbH, Freiburg, Germany: LCI-100C Inertial Measurement Unit (2013). Data sheet
47. Pellman, E.J., Viano, D.C., Withnall, C., Shewchenko, N., Bir, C.A., Halstead, P.D.: Concussion in professional football: helmet testing to assess impact performancepart 11. Neurosurgery **58**(1), 78–95 (2006)

48. Prikhodko, I.P., Zotov, S.A., Trusov, A.A., Shkel, A.M.: What is mems gyrocompassing? comparative analysis of maytagging and carouseling. Journal of Microelectromechanical Systems **22**(6), 1257–1266 (2013). DOI 10.1109/JMEMS.2013.2282936
49. Read, J., Martino, L., Hollmn, J.: Multi-label methods for prediction with sequential data. Pattern Recognition **63**, 45 – 55 (2017). DOI http://dx.doi.org/10.1016/j.patcog.2016.09.015. URL http://www.sciencedirect.com/science/article/pii/S0031320316302758
50. Ren, M., Pan, K., Liu, Y., Guo, H., Zhang, X., Wang, P.: A novel pedestrian navigation algorithm for a foot-mounted inertial-sensor-based system. Sensors **16**(1) (2016). DOI 10.3390/s16010139
51. Roetenberg, D., Luinge, H., Slycke, P.: Xsens MVN: Full 6DOF human motion tracking using miniature inertial sensors. Tech. rep., Xsens Motion Technologies BV (2009)
52. Rong, L., Zhiguo, D., Jianzhong, Z., Ming, L.: Identification of individual walking patterns using gait acceleration. In: 2007 1st International Conference on Bioinformatics and Biomedical Engineering, pp. 543–546 (2007)
53. Rothman, Y., Klein, I., Filin, S.: Analytical observability analysis of ins with vehicle constraints. Navigation **61**(3), 227–236 (2014). DOI 10.1002/navi.63. URL http://dx.doi.org/10.1002/navi.63. NAVI-2014-006.R1
54. Savage, P.: Strapdown inertial navigation integration algorithm design. Journal of Guidance, Control and Dynamics **21**(1-2) (1998)
55. Savage, P.G.: Laser gyros in strapdown inertial navigation systems. In: Proc. IEEE Position, Location, and Navigation Symp. San Diego, CA (1976)
56. Sierociuk, D., Tejado, I., Vinagre, B.M.: Improved fractional Kalman filter and its application to estimation over lossy networks. Signal Process. **91**(3), 542–552 (2011)
57. Skog, I., Händel, P., Nilsson, J.O., Rantakokko, J.: Zero-velocity detection—an algorithm evaluation. IEEE Transactions on Biomedical Engineering **57**(11), 2657–2666 (2010). DOI 10.1109/TBME.2010.2060723
58. Skog, I., Nilsson, J.O., Hndel, P., Nehorai, A.: Inertial sensor arrays, maximum likelihood, and cramer-rao bound. IEEE Transactions on Signal Processing **64**(16), 4218–4227 (2016). DOI 10.1109/TSP.2016.2560136
59. STMicroelectronics: LSM6DSL iNEMO inertial module: always-on 3D accelerometer and 3D gyroscope (2017). Data sheet rev. 7
60. Titterton, D.H., Weston, J.L.: Strapdown Inertial Navigation Technology, 2nd edn. American Institute of Aeronautics and Astronautics, Reston, VA (2004)
61. Tweed, D.B., Haslwanter, T.P., Happe, V., Fetter, M.: Non-commutativity in the brain. Nature **399**(6733), 261–263 (1999)
62. Twomey, N., Diethe, T., Kull, M., Song, H., Camplani, M., Hannuna, S., Fafoutis, X., Zhu, N., Woznowski, P., Flach, P., Craddock, I.: The SPHERE challenge: Activity recognition with multimodal sensor data. arXiv preprint arXiv:1603.00797 (2016)
63. Voisin, M., Dreyfus-Schmidt, L., Gutierrez, P., Ronsin, S., Beillevaire, M.: Dataiku's solution to sphere's activity recognition challenge (2016)
64. Voss, R.F.: $1/f$ (flicker) noise: A brief review. In: Proc. 33rd Ann. Symp. Frequency Control, pp. 40–46 (1979)
65. Webb, A.: Statistical Pattern Recognition, 2nd edn. John Wiley & Sons, LTD (2002)
66. Woodman, O., Harle, R.: Pedestrian localisation for indoor environments. In: Proceedings of the 10th International Conference on Ubiquitous Computing, UbiComp '08, pp. 114–123. ACM, New York, NY, USA (2008). DOI 10.1145/1409635.1409651. URL http://doi.acm.org/10.1145/1409635.1409651
67. Xsens MVN – inertial motion capture. URL http://www.xsens.com/en/general/mvn
68. Yu, J., Chen, Z., Zhu, Y., Chen, Y., Kong, L., Li, M.: Fine-grained abnormal driving behaviors detection and identification with smartphones. IEEE Transactions on Mobile Computing (2016). DOI 10.1109/TMC.2016.2618873
69. Zhang, M.L., Zhou, Z.H.: A review on multi-label learning algorithms. IEEE Transactions on Knowledge and Data Engineering **26**(8), 1819–1837 (2014). DOI 10.1109/TKDE.2013.39